VOLUME 7, NUMBER 12, DECEMBER 2007

NANO LETTERS

Preparation of Radial and Longitudinal Nanosized Heterostructures of In_2O_3 and SnO_2

A. Vomiero,*,†,‡ M. Ferroni,†,‡ E. Comini,†,‡ G. Faglia,†,‡ and G. Sberveglieri†,‡

INFM-CNR Sensor Lab, Via Valotti 9, 25133 Brescia, Italy, and Department of Chemistry and Physics for Engineering and Materials, University of Brescia, Via Valotti 9, 25133 Brescia, Italy

Received June 5, 2007; Revised Manuscript Received October 8, 2007

ABSTRACT

Radial and longitudinal nanosized In_2O_3–SnO_2 heterostructures were produced by applying a suitable methodology of transport and condensation. Sequential evaporation–condensation over In-seeded alumina promotes the formation of a radial heterostructure, driven by the direct vapor–solid growth mechanism. The single-crystalline In_2O_3 nanowire nucleates and acts as the backbone for condensation of a polycrystalline SnO_2 sheath. Fabrication of longitudinal heterostructures over sapphire is achieved through the application of a nanosized gold catalyst: the gold particles promote nucleation according to the vapor–liquid–solid mechanism, and lead to the formation of single-crystalline In_2O_3 nanowires with a gold droplet at the apex. Gold maintains its catalytic activity even during subsequent evaporation of SnO_2 and induces the nucleation of a SnO_2 single-crystal nanowire from the termination of an In_2O_3 nanowire. The electrical characterization of the longitudinally assembled In_2O_3–SnO_2 structure highlighted a peculiar behavior, as the heterojunction of two *n*-type semiconducting oxides was revealed, tin oxide being reversely biased. These results hold great potential for the application of precisely shaped heterojunctions.

The increasing scientific interest in quasi one-dimensional (1-D) systems such as nanowires and nanorods has stimulated their functional exploitation, and single-crystalline 1-D nanostructures are nowadays emerging as building blocks for a new generation of electronic[1−3] and optoelectronic nanometer-scaled devices.[4,5] The fabrication techniques of homogeneous 1-D nanostructures have pursued the control over shape, aspect-ratio, and crystalline arrangement to a considerable degree, and the improvement of the synthesis methods[6] has recently achieved the direct integration of functional nanostructures into nanodevices. A series of nanoprototypes has been demonstrated, such as single GaN nanowire field-effect transistors,[3] passive diodes, active bipolar transistors and complementary inverted-like structures[1,2] using a crossed-wire design, and single-crystalline branched nanowires.[7]

In the field of ionic metal oxides, the structural and functional properties of 1-D nanostructures and their great functional potential are attracting almost the same consideration addressed to covalent 1-D nanostructures based on either silicon or group III−V compounds.[8,9] Crystalline nanowires of metal-oxides have been investigated, starting

* Corresponding author. E-mail: alberto.vomiero@ing.unibs.it; fax: +39 030 2091 271.
† INFM-CNR Sensor Lab.
‡ University of Brescia.

10.1021/nl071339n CCC: $37.00
Published on Web 11/15/2007

from the work of Wang and co-workers,[10] and a series of different materials[11] have been produced, for example, ZnO,[12] SnO_2,[13] MgO,[14] SiO_2,[15] and In_2O_3.[16,17]

Further improvement of the preparation methodologies addresses the capability to fabricate heterogeneous structures and chemically nonhomogeneous 1-D nanostructures with novel functional properties.[18] The key step for device fabrication is the transition from self-organized structures to patterned assembling (a wide review on the topic is reported in ref 19). Different approaches and preparation methodologies have been implemented for this purpose, and several systems have been described in the literature up to now: parallel core−shell metal dielectric semiconductor nanowires,[20] core−shell metallic nanowires and nanotubes,[21] or the axially modulated doping of Si nanowires,[22] silicon, and metallic wires modified by an electron beam.[23] Research is also developing the controlled growth of multiple wire types and ternary compounds.[24] Self-assembled branched structures have been obtained very recently via the catalyzed epitaxial growth of oxide nanowires on suitably seeded backbones.[25]

While superlattices of different III−V semiconductors have been synthesized,[26] and selective doping of single oxide nanowire has been carried out for the creation of a nanojunction,[27] no systematic progress has been gained on the synthesis of 1-D heterostructures composed of two oxides. Such a junction may allow exploitation of the different intrinsic electronic band-structures of each oxide in fields such as Shottky-like barrier diode gas sensors,[28] solar cells,[29] and lithium ion batteries.[30]

The present work reports on the fabrication of In_2O_3−SnO_2 nanosized systems, assembled in either radial or linear heterostructures. The capability to tailor the morphology, the crystallinity, and the composition of the heterostructures through rational control of the evaporation−condensation parameters and the usage of a catalyst will be demonstrated.

As schematically shown in Figure 1a, the vapor−solid (VS) process[31] was used to fabricate a radial In_2O_3−SnO_2 heterostructure. The In_2O_3−SnO_2 radial heterostructure was obtained starting from crystalline In_2O_3 nanowires prepared on alumina substrate. Second, the condensation of SnO_2 was carried out, accomplishing the formation of the heterostructure with In_2O_3 nanowires as the backbone. In order to control the size of the nanowires and allow a patterning capability, the substrate was preliminarily seeded with indium nanoparticles.[32] No catalyst metal was therefore used for preparation of the radial heterostructure: this approach relies on the VS process as the main mechanism for the synthesis and guarantees the achievement of a highly pure and catalyst-free nanostructure.

The advantage offered by metal catalysts for the fabrication of nanowires[8,33] has been used for the longitudinal assembling of the heterostructure (see Figure 1b). In fact, the sapphire substrate was preliminarily seeded with gold nanoparticles. In this case, In_2O_3 nanowires were produced via the vapor−liquid−solid (VLS) mechanism. As the gold droplet located at the apex of the In_2O_3 nanowire, Au effectively promotes the nucleation of the SnO_2 nanowire during the second condensation step. Nucleation of indium and tin oxide nanowires occurs at 800 °C and 600 °C, respectively. Precise control of both the condensation conditions and the growth rate, as well as proper seeding of the substrate, are required[32] for obtaining indium and tin oxide nanowires with similar size.

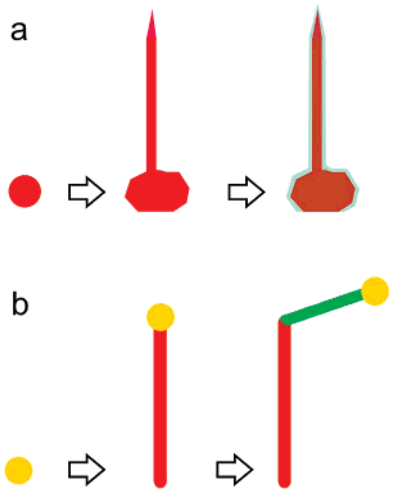

Figure 1. (a) Schematic of the VS growth of radial heterostructure (not to scale). In_2O_3 nanowire (red) nucleates from the oxidized In seed over the alumina substrate, then coverage with tin oxide (green) is pursued. The duration for the second step results in partial coverage of the nanowire and eventually accomplishes formation of the radial heterostructure. (b) VLS growth of longitudinal heterostructures (not to scale). The growth of an In_2O_3 nanowire (red) is catalyzed by Au nanoparticles (yellow) on a sapphire substrate. The Au particle at the apex of the In_2O_3 nanowire also promotes the nucleation of a SnO_2 nanowire (green) during the second condensation step, leading to formation of the longitudinal heterostructure.

For the radial heterostructures, an In buffer layer (5 nm nominal thickness) was preliminarily deposited on an alumina substrate by direct current sputtering. Decomposition of In_2O_3 precursor powders (99.99% purity) took place in a tubular furnace at a temperature of 1500 °C. The condensation occurred at a temperature between 750 and 900 °C downstream from the constant Ar flow (50 sccm). During transient heating of the furnace, metallic indium nanoparticles oxidized to form In_2O_3 micrograins, acting as effective seeds for nanowire nucleation. As shown in Figure 2, 1 h of condensation led to the growth of single-crystalline wires, tens of microns in length. The lateral dimension of the In_2O_3 nanowires ranged between 40 and 300 nm, and the size distribution is presented in Figure 2. It turns out that the preliminary indium seeding of the substrate is fundamental in narrowing and reducing the size of the In_2O_3 nanowires.

The condensation process was repeated starting from the SnO_2 precursor (99.99% purity). Oxidized tin was nucleated over an In_2O_3 nanowire, which serves as the backbone for the radial heterostructures. The duration of SnO_2 deposition discriminated the formation of a radial SnO_2−In_2O_3 heterostructure, with the In_2O_3 nanowire fully or partially covered by tin oxide. The diameter of the radial heterojunction, after short SnO_2 condensation, ranged between 150 and 300 nm.

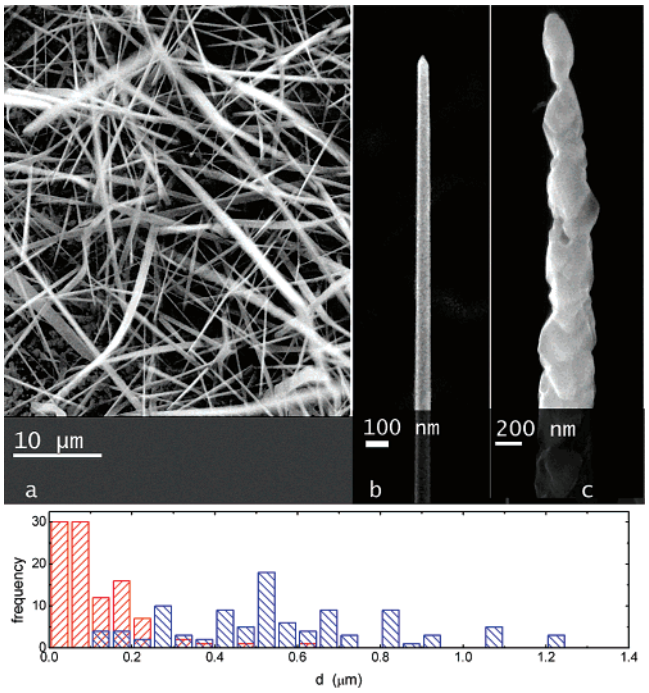

Figure 2. Secondary-electron scanning electron microscopy (SEM) images of radial heterostructures. (a) In_2O_3 nanowire bundle after the VS growth and (b) detail of a single In_2O_3 nanowire (60 nm in width). (c) In_2O_3 nanowire completely decorated by SnO_2 after a 20-min condensation. (Bottom) Comparison of the lateral size distribution of the nanowires grown on In-seeded (red) and unseeded (blue) substrate.

Subsequent long-time condensation (20 min) of SnO_2 on In_2O_3 nanowires (Figure 2c) completed the SnO_2 sheath.

Figure 3a,b shows the morphology and the elemental distribution of tin and indium in a radial heterostructure. Indium is present over the entire structure, while no presence of Sn was recorded in the central part. This evidence indicates that tin oxide nucleates at different positions along the nanowire and that the SnO_2 crystalline domains develop symmetrically along the indium oxide backbone, as schematically illustrated in Figure 4. In the early stage of condensation, nucleation of crystalline SnO_2 domains occurred as a result of epitaxial growth on the In_2O_3 single crystal. Eventually, lattice mismatch between the cubic In_2O_3 and the tetragonal SnO_2 lattices constrains the size of the grains and results in polycrystalline coverage. After long-time SnO_2 condensation, SnO_2 completely encircles the In_2O_3 core. Indeed, the transverse energy-dispersive X-ray (EDX) line-scan of the distribution of In and Sn (Figure 3e) reveals that In peaks in the inner part of the heterostructure and that Sn is radially distributed. The broadening of the signals is due to the spreading of the electron beam. The presence of contaminants is excluded within the sensitivity of EDX.

Figure 5 summarizes the results on the structural characterization by transmission electron microscopy (TEM). The compositional image provided by scanning TEM high angle annular dark field (STEM-HAADF) imaging highlights the inner In_2O_3 nanowire. Tin oxide condensed in the form of polycrystals, as visible because of the fine contrast variations in both TEM and STEM-HAADF images. Lateral dimensions of SnO_2 crystalline domains are about 50 nm. The selected area electron diffraction (SAED) pattern shows that the nanowire exhibits monocrystalline arrangement, with Bragg reflections fitted by the cubic phase of In_2O_3. The nanowire is oriented in the [100] direction of the crystal lattice. The reflections pertaining to tin oxide are not systematically arranged, but, in this case, the (101) reciprocal lattice vectors are aligned with the (321) direction of In_2O_3. This evidence indicates that the monocrystalline arrangement of the In_2O_3 backbone drives the crystallization of some tin oxide domains with a specific orientation relationship to the lattice of In_2O_3, and supports the proposed model for ordered assembling of the radial heterostructure.

As far as the linear heterostructures are concerned, Figure 6 shows that gold-seeded sapphire promotes the growth of

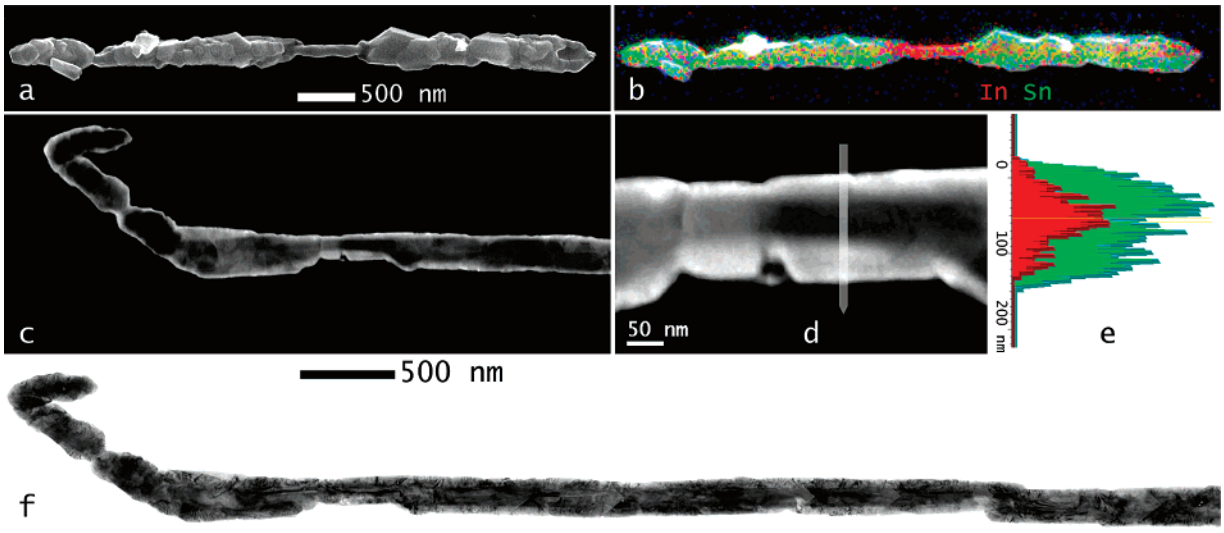

Figure 3. Compositional analysis of radial heterostructures: (a) secondary-electron image of the heterostructure; (b) the corresponding EDX colored map for indium (red) and tin (green); (c) the STEM image of a radial heterostructure, revealing the presence of a inner dark core along the structure; (d−e) STEM image at higher magnification and the transverse EDX line-scan showing the indium-based core; (f) TEM panoramic view of the same heterostructure, highlighting the polycrystalline arrangement of the SnO_2 sheath.

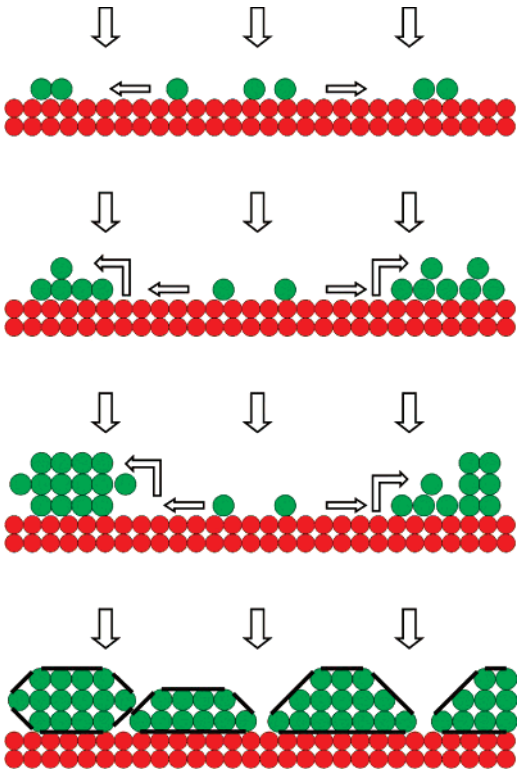

Figure 4. Model for the condensation of SnO_2 polycrystals over the lateral sides of the In_2O_3 single-crystal nanowire. The early ordered arrangement of SnO_2 is driven by epitaxial growth.

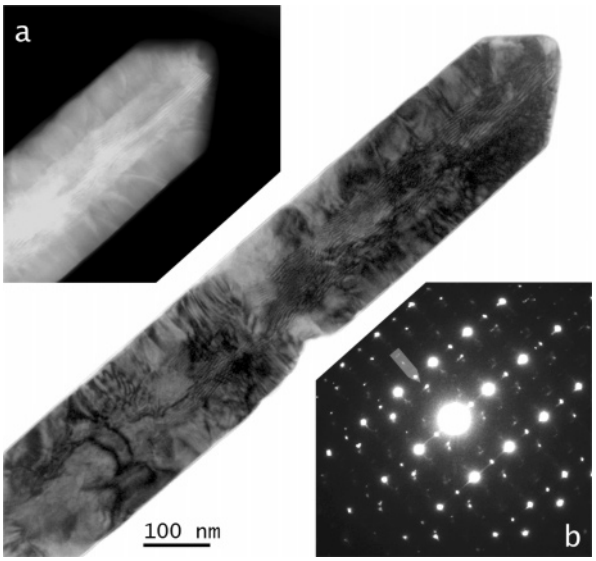

Figure 5. Structural characterization of a radial heterostructure. (Main Picture) TEM image of the heterostructure, in which the contrast variations reveal the polycrystalline arrangement for tin oxide. (a) STEM-HAADF compositional image of the apex. The bright contrast of the inner core highlights the In_2O_3 nanowire. (b) SAED pattern of the heterostructure. The systematic rows of Bragg reflections pertain to the cubic phase of In_2O_3. Extra reflections are attributed to SnO_2, with a specific orientation relationship to the lattice of In_2O_3. The arrow marks the common direction shared by the (110) and (321) Bragg reflections of tin and indium oxides, respectively.

In_2O_3 single-crystal nanowires, with preferential orientation normal to the substrate. The conical shape of the In_2O_3 nanowires is due to the slow reduction of the size of the Au

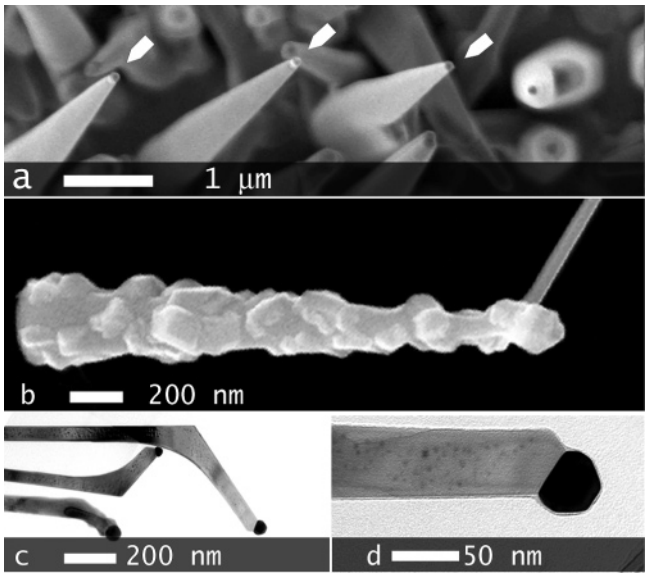

Figure 6. Morphological characterization of longitudinal heterostructures. (a) SEM image of the In_2O_3 nanowires produced by VLS growth; each wire is terminated by a gold nanoparticle (arrows). (b) SEM image of In_2O_3 nanowire with the SnO_2 nanowire originating from its apex. (c) TEM image of the termination of SnO_2 nanowires with catalytic Au particles. (d) TEM image of the crystalline SnO_2 nanowire and the faceted Au nanoparticle.

catalyst during condensation at 900 °C. A single-crystalline tin oxide nanowire originates from the catalytic Au particle at the end of the In_2O_3 nanowire. A beak-like structure terminates each nanowire, and is caused by the cooling transient at the end of the condensation process, according to ref 34. In addition to the formation of the linear heterostructure, multiple condensation of tin oxide polycrystals on the lateral sides of In_2O_3 nanowire still occurs, but it is of minor importance with respect to the growth of the nanowire because of its very high rate of growth (~500 nm/s). According to the VLS mechanism, the diameter of the Au catalyst determines the lateral dimensions of both In_2O_3 and SnO_2 nanowires.

TEM imaging, carried out along different zones of the heterojunction, and the complementary SAED and convergent beam electron diffraction (CBED) analyses (Figure 7) show the cubic single-crystalline arrangement of an In_2O_3 nanowire (Figure 7, area 1), which grows along the [110] direction, in agreement with the results of ref 16; the single-crystal tetragonal (cassiterite) arrangement of a tin oxide nanowire along the [101] direction (Figure 7, area 2); the simultaneous presence of crystalline In_2O_3 and SnO_2 crystal lattices in the region of the junction; and the sharp interface between indium oxide and tin oxide nanowires (Figure 7, areas 3 and 4).

Typically, charge carriers in metal oxides are generated by structural defects, mainly ionized oxygen vacancies and cation interstitials, and the material features a high density of electronic states and behaves as a wide band gap semiconductor.[35]

Figure 8 reports the $I-V$ characteristic of a double-isotype *n*-type heterojunction formed by SnO_2 (polycrystals)$-In_2O_3$ (nanowire)$-SnO_2$ (nanowire). The applied voltage drops in

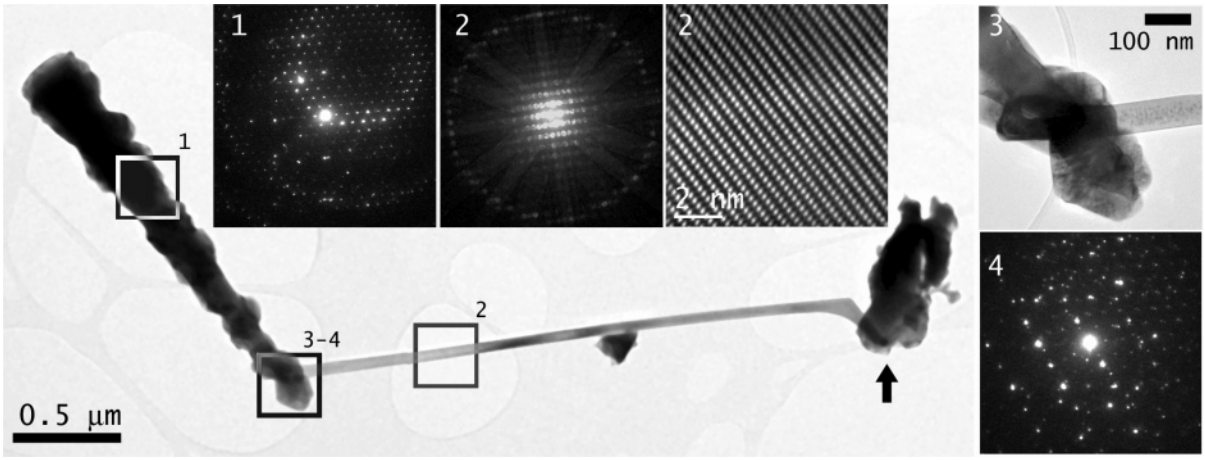

Figure 7. Structural characterization of longitudinal heterostructures. (Main Picture) TEM panoramic view of the In_2O_3 nanowire, with the SnO_2 nanowire extending lengthwise. The black arrow marks the termination of the SnO_2 nanowire and the catalytic Au nanoparticle, which assisted the VLS growth of heterostructure. (1) SAED pattern showing the cubic single-crystal arrangement for the indium oxide nanowire. (2) CBED pattern and high-resolution image from the tin oxide nanowire, demonstrating its single-crystalline tetragonal (cassiterite) arrangement. (3,4) highly magnified TEM view and corresponding SAED pattern of the heterojunction, where superimposition of both indium and tin oxides has been recorded.

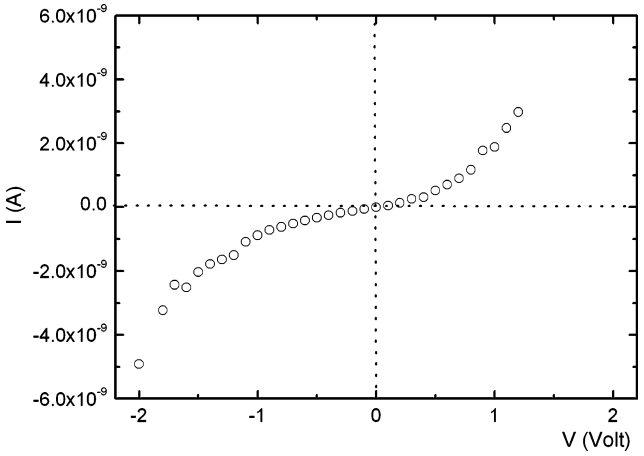

Figure 8. Current−voltage characteristic of the SnO_2 (polycrystals)−In_2O_3 (nanowire)−SnO_2 (nanowire) heterojunction measured by two piezo-actuated nanoprobes inside the SEM.

the reverse biased heterojunction, which is asymmetric for positive and negative voltages; the slightly rectifying behavior has to be ascribed to the different shape and crystalline state of the SnO_2 for the two heterojunctions. In the voltage range between −0.5 and 0.5 V, the current−voltage relationship is compatible with the presence of an inverse saturation current, which, for *n*-type heterojunctions, depends linearly on the applied voltage.[36] As the inverse current is also linearly dependent on the temperature, the $I-V$ deviation from linearity at higher applied voltages is ascribable to self-heating effects.

In summary, the ability of fabricating axial core−shell and linear metal-oxide heterojunctions, and effective rational control of the entire growth process was demonstrated. The critical parameter leading the formation of different shapes is the presence of active catalysts driving the nucleation mechanism.

Single-crystalline In_2O_3 nanowires were obtained by the VS process through seeding with metallic indium the alumina substrate and controlling the lateral dimension of In_2O_3 nanowires serving as the backbone for radial heterostructures. During repeated evaporation, volatile species from SnO_2 powders condensate on the In_2O_3 backbone in the form of polycrystalline domains, and lead to partial or full coverage of In_2O_3 nanowires, depending on the duration of the condensation process. Condensation time also determines the thickness of the SnO_2 layer. The epitaxial relationship between the indium oxide and tin oxide lattices in the early stage of the formation of the heterostructure was recorded.

Differently, the presence of gold catalyst on sapphire substrate results in the oriented growth of In_2O_3 nanowires according to the VLS mechanism. The crystalline Au particle assists the VLS growth of both indium and tin oxide nanowires. The preservation of this catalytic activity is fundamental for obtaining the linear heterostructures. Similar methodology was applied for the fabrication of gallium arsenide/gallium phosphide superlattices, but it has never been reported for oxides.[37] During the sequential evaporation of SnO_2, gold droplets act as preferential sites for the nucleation and growth of single-crystalline SnO_2 nanowires. This self-assembly methodology proved effective for obtaining linear heterojunctions with precise spatial control of the position of SnO_2 nanowires, overcoming the drawback of nucleation of disordered hierarchical heterostructures, which is typical of the sequential seeding of an active catalyst.[7]

Electrical characterization of a single SnO_2(polycrystals)−In_2O_3−SnO_2 structure indicates the presence of a heterojunction of two *n*-type semiconducting oxides, and forecasts the technological exploitation of the interface properties.

Acknowledgment. The work was partially funded by the European Commission (*Nanostructured solid-state gas sensors with superior performance*-NANOS4 STREP Project No. NMP 001528), and MIUR (*Quasi mono dimensional nanosensors for label free ultra sensitive biological detection* PRIN Project 2005).

References

(1) Cui, Y.; Lieber, C. M. *Science* **2006**, *291*, 851.
(2) Duan, X.; Huang, Y.; Cui, Y.; Wang, J.; Lieber, C. M. *Nature* **2001**, *409*, 66.
(3) Huang, Y.; Duan, X.; Cui, Y.; Lieber, C. M. *Nano Lett.* **2002**, *2*, 101.
(4) Lieber, C. M. *MRS Bull.* **2003**, *28*, 486.
(5) Samuelson, L. *Mater. Today* **2003**, *6*, 22.
(6) Stellacci, F. *Adv. Funct. Mater.* **2006**, *16*, 15.
(7) Jung, Y.; Ko, D.-K.; Agarwal, R. *Nano Lett.* **2006**, *7*, 264.
(8) Wan, Q.; Dattoli, E. N.; Fung, W. Y.; Guo, W.; Chen, Y.; Pan, X.; Lu, W. *Nano Lett.* **2006**, *6*, 2909.
(9) Lu, J. G.; Chang, P.; Fan, Z. *Mater. Sci. Eng., R* **2006**, *52*, 49.
(10) Pan, Z. W.; Dai, Z. R.; Wang, Z. L. *Science* **2001**, *291*, 1947.
(11) Xia, Y.; Yang, P.; Sun, Y.; Wu, Y.; Mayers, B.; Gates, B.; Yin, Y.; Kim, F.; Yan, H. *Adv. Mater.* **2003**, *15*, 353.
(12) Wang, Z. L. *J. Phys.: Condens. Matter* **2004**, *16*, R829.
(13) Calestani, D.; Zha, M.; Salviati, G.; Lazzarini, L.; Zanotti, L.; Comini, E.; Sberveglieri, G. *J. Cryst. Growth* **2005**, *275*, e2083.
(14) Yang, P.; Lieber, C. M. *Science* **1996**, *273*, 1836.
(15) Wang, Z. L.; Gao, R. P.; Gole, J. L.; Stout, J. D. *Adv. Mater.* **2000**, *12*, 1938.
(16) Nguyen, P.; Ng, H. T.; Yamada, T.; Smith, M. K.; Li, J.; Han, J.; Meyyappan, M. *Nano Lett.* **2004**, *4*, 651.
(17) Liang, C.; Meng, G.; Lei, Y.; Phillipp, F.; Zhang, L. *Adv. Mater.* **2001**, *13*, 1330.
(18) Functional Nanowires (Special Issue). *MRS Bull.* **2007**, *32* (issue 2).
(19) Fan, H. J.; Werner, P.; Zacharias, M. *Small* **2006**, *2*, 700.
(20) Zhang, L.; Tu, R.; Dai, H. *Nano Lett.* **2006**, *6*, 2785.
(21) Li, L.; Yang, Y.-W.; Li, G.-H.; Zhang, L.-D. *Small* **2006**, *2*, 548.
(22) Yang, C.; Barrelet, C. J.; Capasso, F.; Lieber, C. M. *Nano Lett.* **2006**, *6*, 2929.
(23) Xu, S.; Tian, M.; Wang, J.; Xu, J.; Redwing, J. M.; Chan, M. H. W. *Small* **2005**, *1*, 1221.
(24) Johnson, M. C.; Aloni, S.; McCready, D. E.; Bourret-Courchesne, E. *Cryst. Growth Des.* **2006**, *6*, 1936.
(25) Wan, Q.; Wei, M.; Zhi, D.; MacManus-Driscoll, J. L.; Blamire, M. G. *Adv. Mater.* **2006**, *18*, 234.
(26) (a) Wu, Y.; Fan, R.; Yang, P. *Nano Lett.* **2002**, *2*, 83. (b) Björk, M. T.; Ohlsson, B. J.; Sass, T.; Persson, A. I.; Thelander, C.; Magnusson, M. H.; Deppert, K.; Wallenberg, L. R.; Samuelson, L. *Nano Lett.* **2002**, *2*, 87.
(27) Pradhan, B.; Batabyal, S. K.; Pal, A. J. *Appl. Phys. Lett.* **2006**, *89*, 233109.
(28) Madou, M. J.; Morrison, S. R. *Chemical Sensing with Solid State Devices*; Academic Press: San Diego, CA, 1989; p 420.
(29) Law, M.; Greene, L. E.; Radenovic, A.; Kuykendall, T.; Liphardt, J.; Yang, P. *J. Phys. Chem. B* **2006**, *110*, 22652.
(30) Kim, D.-W.; Hwang, I.-S.; Kwon, S. J.; Kang, H.-Y.; Park, K.-S.; Choi, Y.-J.; Choi, K.-J.; Park J.-G. *Nano Lett.* **2007**, *7*, 3041.
(31) (a) Burton, W. K.; Cabrera, N.; Frank, F. C. *Philos. Trans. R. Soc.* **1951**, *243*, 299. (b) Zhang, H. Z.; Kong, Y. C.; Wang, Y. Z.; Du, X.; Bai, Z. G.; Wang, J. J.; Yu, D. P.; Ding, Y.; Hang, Q. L.; Feng, S. Q. *Solid State Commun.* **1999**, *109*, 677. (c) Cui, Z.; Meng, G. W.; Huang, W. D.; Wang, G. Z.; Zhang, L. D. *Mater. Res. Bull.* **2000**, *35*, 1653.
(32) Vomiero, A.; Bianchi, S.; Comini, E.; Faglia, G.; Ferroni, M.; Sberveglieri, G. *Cryst. Growth Des.*, in press.
(33) Cao, G. *Nanostructures & Nanomaterials*; Imperial College Press: London, 2004.
(34) He, J. H.; Wu, T. H.; Hsin, C. L.; Li, K. M.; Chen, L. J.; Chueh, Y. L.; Chou, L. J.; Wang, Z. L. *Small* **2006**, *2*, 116.
(35) Li, C.; Zhang, D. H.; Han, S.; Liu, X. L.; Tang, T.; Zhou, C. W. *Adv. Mater.* **2003**, *15*, 143.
(36) Sze, S. M. *Physics of Semiconductor Devices*, 2nd ed.; John Wiley and Sons: New York, 1981; pp 122−126.
(37) Gudiksen, M. S.; Lauhon, L. J.; Wang, J.; Smith, D.; Lieber, C. M. *Nature* **2002**, *415*, 617.

NL071339N